Smart Structures and Systems, Vol. 10, No. 6 (2012) 557-572
DOI: http://dx.doi.org/10.12989/sss.2012.10.6.557

Semi-active control on long-span reticulated steel structures using MR dampers under multi-dimensional earthquake excitations

Zhen Zhou*, Shao-ping Meng, Jing Wu and Yong Zhao

Southeast University, Key Laboratory of Concrete and Prestressed Concrete Structures of the Ministry of Education, Nanjing, 210096, China

(Received January 15, 2012, Revised June 27, 2012, Accepted October 3, 2012)

Abstract. This paper focuses on the vibration control of long-span reticulated steel structures under multi-dimensional earthquake excitation. The control system and strategy are constructed based on Magneto-Rheological (MR) dampers. The LQR and Hrovat controlling algorithm is adopted to determine optimal MR damping force, while the modified Bingham model (MBM) and inverse neural network (INN) is proposed to solve the real-time controlling current. Three typical long-span reticulated structural systems are detailedly analyzed, including the double-layer cylindrical reticulated shell, single-layer spherical reticulated shell, and cable suspended arch-truss structure. Results show that the proposed control strategy can reduce the displacement and acceleration effectively for three typical structural systems. The displacement control effect under the earthquake excitation with different PGA is similar, while for the cable suspended arch-truss, the acceleration control effect increase distinctly with the earthquake excitation intensity. Moreover, for the cable suspended arch-truss, the strand stress variation can also be effectively reduced by the MR dampers, which is very important for this kind of structure to ensure that the cable would not be destroyed or relaxed.

Keywords: vibration control; reticulated steel structure; MR damper; semi-active control; earthquake excitation

1. Introduction

With the development of the economy and the construction technology, there have been great improvements in long-span reticulated steel structures for their reasonable structural system, strong spanning ability and spatial diversity. They are widely used in the public buildings such as gymnasiums, museums, opera houses, waiting halls and industrial constructions like long-span workshops and airplane hangars. At present, the reticulated steel structure has various kinds of styles, including traditional structural systems such as cylindrical or spherical reticulated shells (Shen *et al.* 2004, Fan *et al.* 2010, Lopez *et al.* 2007), and a few cable-stayed structures, such as cable suspended arch-truss (Saitoh *et al.* 1999, Wu 2008, Xue *et al*. 2009).

The researches of the Northridge and Kobe earthquake showed that long-span steel structure could also be destroyed severely in the high intensity earthquake (Michel 1995). How to reduce the seismic response of them obtains more and more emphasis of scholars and engineers. Up to now, there have

*Corresponding author, Dr., E-mail: seuhj@163.com

been many researches about the passive control on the long-span steel structures. Motohiko *et al.* (1996) used TMD system to reduce the response of the long span spatial structure under the earthquake. Iwata *et al.* (1999) put several viscoelastic dampers to the base of the reticulated shell to absorb the earthquake energy and reduce the structural seismic response. For the limited control range and effect of passive control method, some scholars focused on the semi-active and intelligent control. Onoda *et al.* (1996) studied the semi-active control in the space truss structure with the electro-rheological damper and results showed that this kind of control strategy is effective and applicable. Zhang *et al.* (2001) developed a theory that some bottom chords are replaced with controllable chords to conduct semi-active control strategy in reticulated shell structures.

In recent years, the magneto-rheological (MR) damper has become one of the most successful semi-active control methods, and has attracted much attention of many scholars and engineers. Some experiment studies has shown that MR dampers can effectively control the structural response under earthquake excitations, and the proposed control algorithm can be simulated effectively by the numerical analysis (Dominguez *et al.* 2008, Wu *et al*. 2010, Yang *et al.* 2011). More researches adopted numerical analysis to investigate the semi-active control effect using MR dampers for various kinds of multi-storey or bridge structures (Huang *et al.* 2012, Jung *et al.* 2008, Ying *et al.* 2009, Kim *et al.* 2011, Bitaraf *et al.* 2010, Erkus *et al.* 2002). However, there are few researches on the seismic control of long-span reticulated steel structures based on MR dampers. In this paper, the long-span reticulated structures are taken as controlled system based on MR dampers. The LQR and Hrovat controlling algorithm is adopted to determine optimal MR damping force, while the modified Bingham model (MBM) and inverse neural network (INN) is proposed to solve the real-time controlling current. Three typical long-span reticulated structural systems are detailedly analyzed under multi-dimensional earthquake excitation.

2. Mechanical model of MR dampers

2.1. Modified bingham model

The mechanical model which is generally used for MR dampers includes the Bingham model and Bouc-Wen hysterisis model. Bingham model can fit well the force-displacement response of MR dampers, while not efficient for the nonlinear response of force-velocity, especially when the velocity is very small and the displacement is in the same direction with the velocity. Bouc-Wen hysterisis model introduces two inner variables and constructs a differential equation model including 14 parameters, which can fit well the experimental data. However, this model is very complex and involves many parameters, and moreover the physical concept is not very clear. In this paper, based on Bingham model and considering the three-stage constitutive relation of pre-yielding, yielding and post-yielding, a modified Bingham model (MBM) is adopted, which can not only describe the character of MR dampers under time-dependent current, but also possess a relatively simple formulation and fewer parameters.

As shown in Fig. 4, MBM is constructed by contacting Bingham element (combined by coulomb friction element and viscosity element) and a spring element. The spring element can be considered as the equivalent axial stiffness including energy accumulator stiffness and the pre-yielding shear modulus of the MR liquid. Then, the damping force of MBM can be expressed as

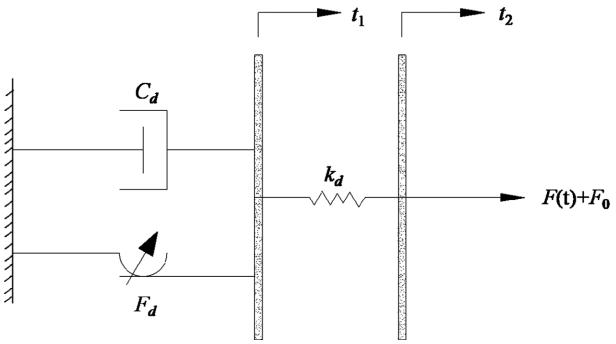

Fig. 1 Construction of MBM (Modified Bingham Model)

$$F(t) = C_d\dot{e} + F_d(E)sgn(\dot{e}) - f_0 = K_d(x-e) - f_0 \tag{1}$$

Where C_d is the viscosity damping coefficient; $F_d(E)$ is the controlling coulomb damping force relevant to the current intensity; e is the displacement of Bingham element; x is the total displacement of the damper; K_d is the equivalent axial stiffness of the damper, relevant to the initial pre-yielding shear modulus and energy accumulator stiffness; f_0 is the output damping force error caused by energy accumulator.

Considering the influence of current intensity on model parameters, C_d, F_d and K_d are all relevant to the current intensity, as following

$$C_d = C_{ds} + C_{dd}u\,,\ F_d = F_{ds}s + F_{dd}u\,,\quad K_d = K_{ds}s + K_{dd}u \tag{2}$$

$$\dot{u} = -\eta(u - I) \tag{3}$$

Where C_{ds}, F_{ds} and K_{ds} are the viscosity damping coefficient, coulomb damping force, and equivalent axial stiffness under zero magnetic field intensity; u is an inner parameter, reflecting the relation of model parameters and current intensity; η reflects the response time of the damper; I denotes the current intensity. Therefore, 8 parameters (C_{ds}, F_{ds}, K_{ds}, C_{dd}, F_{dd}, K_{dd}, f_0, η) should be determined in MBM.

2.2 Inverse neural network for current solving

In the actual control, the current of MR dampers should be solved from the displacement, velocity, and the optimized controlling force. This is an inverse process of the mechanical model of MR dampers. Since the strong nonlinear character of the mechanical model, it is very difficult to establish a mathematical model to describe the inverse dynamic relation between damping force and current. Neural network has been proved to be effective to simulate the model with strong nonlinearity. Therefore, the inverse neural network (INN) model is used to solve the current of dampers in this paper. The control strategy of INN is shown in Fig. 2.

The modeling process of INN needs the displacement, velocity, current and corresponding controlling force solved by the mechanical model of MR dampers, and then the INN is trained with the output is current while the input is displacement, velocity, and controlling force. The essence of INN training process is the input-output mapping described in Eq. (4)

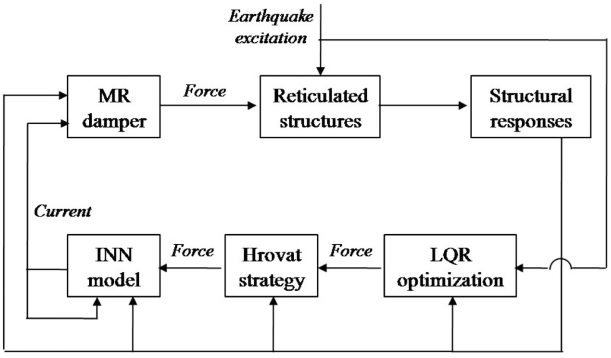

Fig. 2 The control strategy of INN model

$$I(t) = g(\varphi, \theta) \tag{4}$$

Where $I(t)$ is the input current at time t; θ is the weight vector and the weight coefficient is obtained by training. The output vector φ is

$$\varphi(t) = [x(t);x(t-1);x(t-2);F(x);F(x-1);F(x-2)] \tag{5}$$

Where x is the displacement of the damper; F is the damping force.

In this paper, the MBM described in section 2.1 is adopted to produce the forward training data, while the Back Propagation (BP) neural network is used to construct the INN structure. The parameters of MBM is $C_{ds} = 100$ N·s/mm, $F_{ds} = 5400$ N, $K_{ds} = 9000$ N/mm, $C_{dd} = 800$ N·s/mm, $F_{dd} = 4950$ N, $K_{dd} = 8000$ N/mm, $f_0 = 0$ N, $\eta = 167$ s^{-1}. The input and output data is produced by MBM, the sampling frequency is 500 Hz and the sampling time is 10 s. 5000 groups of data are selected, in which the former 2000 groups are used to training INN and the latter 3000 groups are used as testing data. As shown in Fig. 3, the INN is trained through 300 steps and the performance is near 2.45×10^{-5}. Fig. 4

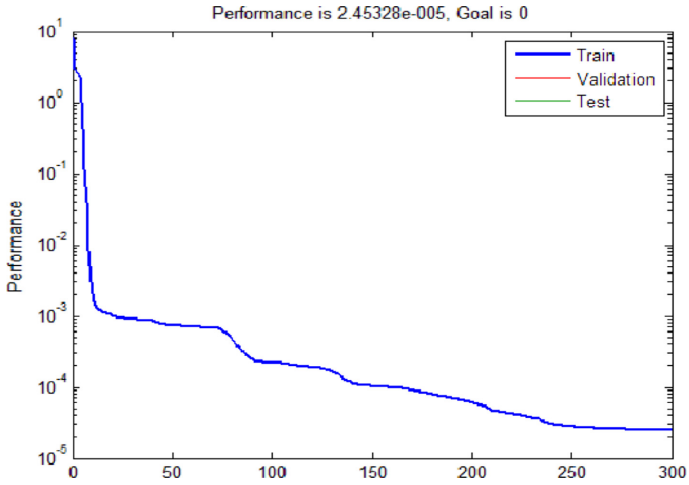

Fig. 3 Training process of INN

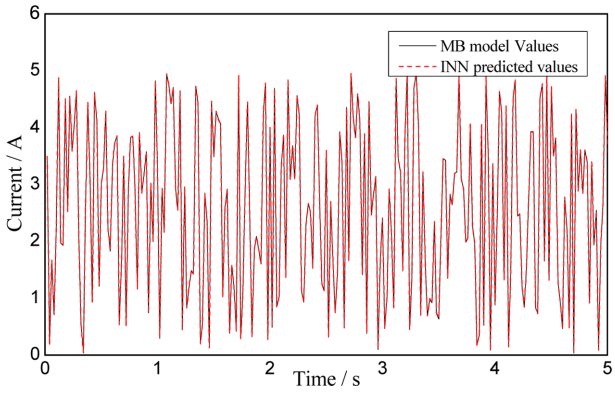

Fig. 4 Prediction results of INN

shows the comparison of MB model values and INN predicted values. It can be seen that the proposed INN model can predict the current accurately according to the displacement of MR dampers.

3. Semi-active control strategy based on LQR

The objective of the control strategy is to determine the real-time control force according to the structural response under seismic excitation. There are some available control methods including linear quadratic regulator (LQR), linear quadratic gaussian (LQG), fuzzy logic control, and sliding model control, etc. Among these methods, LQR control method is the most widely used, because it has been well developed and verified to have stable control effect as well as simple formulations by a great deal of theoretical and experimental research. Therefore, the proposed semi-active control strategy in this paper is constructed based on LQR method.

3.1 Basic equations

The motion equation of long-span reticulated structures under the earthquake can be expressed as following

$$M\ddot{X}+C\dot{X}+KX=-ME_g\ddot{x}_g+B_sU \tag{6}$$

Where, M, C, K are the mass matrix, damp matrix and stiffness matrix of cable-arch structures, respectively; X, $\dot{X}$, $\ddot{X}$ are the vector of the structural displacement, velocity and acceleration, respectively; $\ddot{x}_g$ is the earthquake acceleration; B_s is the controlling force location matrix; U is the vector of the controlling force.

Eq. (6) can be rewritten with the state equation format as following

$$\dot{Z}=AZ+BU+D\ddot{x}_g \tag{7}$$

Where, A is the system matrix, B is the controlling instrument location matrix, D is the vector of the earthquake excitation, as follows

$$A=\begin{bmatrix}0 & I\\ -M^{-1}K & -M^{-1}C\end{bmatrix},\quad B=\begin{bmatrix}0\\ -M^{-1}B_s\end{bmatrix},\quad D=\begin{bmatrix}0\\ E_g\end{bmatrix}$$

The long-span reticulated structure is not the same as the planar high-rise building, since the controlling force provided by MR dampers is spatial, and the three spatial components of the force is relevant to each other, which is also relevant to the angle of MR dampers. Supposing that n dampers are laid on the structure, the position matrix of the controlling force can be describe as following

$$B_s=\begin{bmatrix}
\cos\alpha_1 & & & & \\
\cos\beta_1 & 0 & \cdots & 0 & 0\\
\cos\gamma_1 & & & & \\
 & \cos\alpha_2 & & & \\
0 & \cos\beta_2 & \cdots & 0 & 0\\
 & \cos\gamma_2 & & & \\
\vdots & \vdots & & \vdots & \vdots\\
 & & & \cos\alpha_n & \\
0 & 0 & \cdots & \cos\beta_n & 0\\
 & & & \cos\gamma_n &
\end{bmatrix}$$

Where α, β, γ are the angle of MR dampers in x, y, z direction.

The quadratic form integration of system state Z and controlling input U are selected as the performance index

$$J=\frac{1}{2}\int_{t_0}^{\infty}[Z^TQZ+U^TRU]dt \tag{8}$$

Then, the problem is transformed into: solving the optimum controlling force U to minimization the performance index. According to the Lagrange multiplier method, multiplier vector $\lambda(t)\in R^n$ are introduced, and Eq. (8) are transformed into non-constraint functional extreme value problem. The Lagrange function is as following:

$$L=\int_{t_0}^{\infty}\left[\frac{1}{2}(Z^TQZ+U^TRU)+\lambda^T(AZ+BU-\dot{Z})\right]dt \tag{9}$$

3.2 The optimal control solution

Hamilton function $H(Z, U, \lambda)$ is

$$H(Z,U,\lambda)=\int_{t_0}^{\infty}\left[\frac{1}{2}(Z^TQZ+U^TRU)+\lambda^T(AZ+BU)\right]dt \tag{10}$$

Substitute Eq. (10) into Eq. (9)

$$L=\int_{t_0}^{\infty}[H(Z,U,\lambda)+\dot{\lambda}^TZ]dt-\lambda^TZ\Big|_{t_0}^{\infty} \tag{11}$$

Considering the first order micro, the variational increment relationship can be obtained as

$$\delta L = \delta L_z + \delta L_U + \delta L_\lambda = \int_{t_0}^{\infty} \left[\delta Z^T \left(\frac{\partial H}{\partial Z} + \dot{\lambda} \right) + \delta U^T \frac{\partial H}{\partial U} + \delta \lambda^T \left(\frac{\partial H}{\partial \lambda} - \dot{Z} \right) \right] - \delta Z^T \lambda \Big|_{t_0}^{\infty} \tag{12}$$

For the randomicity of the δZ, δU and $\delta \lambda$, the necessary condition of minimization of function L can be obtained by $\delta L = 0$

$$\frac{\partial H}{\partial Z} + \dot{\lambda} = 0 \quad \frac{\partial H}{\partial U} = 0 \quad \frac{\partial H}{\partial \lambda} - \dot{Z} = 0 \quad \delta Z^T \lambda \Big|_{t_0}^{\infty} = 0 \tag{13}$$

Substitute Eq. (13) into Eqs. (9) and Eq. (10), the following equations can be obtained

$$\dot{\lambda} = -QZ - A^T \lambda \tag{14}$$

$$\frac{\partial H}{\partial U} = RU + B^T \lambda = 0 \tag{15}$$

Since R is positive definite, thus

$$U = -R^{-1} B^T \lambda \tag{16}$$

The linear transformation relation of $\lambda(t)$ and $Z(t)$ can be then established. Suppose

$$\lambda(t) = P(t) Z(t) \tag{17}$$

Substitute Eq. (17) into Eq. (16)

$$U(t) = -R^{-1} B^T P(t) Z(t) \tag{18}$$

The optimal state feedback gain matrix can be obtained as following

$$G = R^{-1} B^T P(t) \tag{19}$$

$$U(t) = -GZ(t) \tag{20}$$

According to Eq. (17)

$$[\dot{P}(t) + P(t)A + A^T P(t) - P(t)BR^{-1}B^T P(t) + Q]Z(t) = 0 \tag{21}$$

For the randomicity of Z, the Riccati equation with P as matrix function is as following

$$\dot{P}(t) + P(t)A + A^T P(t) + P(t)BR^{-1}B^T P(t) + Q = 0 \tag{22}$$

By solving Riccati equation, matrix P can be obtained. The feedback gain matrix G can be solved according to Eq. (19). Finally, the optimal controlling force U can be obtained according to Eq. (20).

3.3 Semi-active controlling algorithm

Since the MR damper supplies the structural damping force by changing the magnetic field intensity, it could not supply the real-time optimal active controlling force solved by Eq. (23), and could only

make the real controlling force close to the theoretically optimal force under maximum available force limit by adjusting the damper parameters. There are three common-used semi-active control algorithms to solve this problem: Bang-Bang, optimal Bang-Bang, and limited Hrovat. Among these three methods, Bang-Bang and optimal Bang-Bang make the control force be only two possible values: maximum or minimum damping force. Limited Hrovat can realize the optimal control force solved by LQR under the limit of minimum and maximum damping force. Therefore, the limited Hrovat controlling algorithm is adopted here to determine the real controlling force provided by MR dampers, as following

$$F_{di}=\begin{cases} c_{ds}\dot{x}_i+f_{d\max}sgn(\dot{x}_i) & (u_i\dot{x}_i>0 \text{且} |u_i|>F_{d\max}) \\ |u_i|sgn(\dot{x}_i) & (u_i\dot{x}_i>0 \text{且} |u_i|>F_{d\max}) \\ c_{ds}\dot{x}_i+f_{d\min}sgn(\dot{x}_i) & (u_i\dot{x}_i\geq 0) \end{cases} \tag{23}$$

Where, $f_{d\max}$ and $f_{d\min}$ are the maximum and minimum damping forces provided by the electrical current; $\dot{x}_i$ is the velocity response of the structure; u_i is the optimal controlling force solved by the LQR control strategy; $c_{ds}\dot{x}_i$ is the viscosity damping force of the MR damper; $F_{d\max}$ is the maximum total damping force of the MR damper.

4. Numerical examples

4.1 Double-layer cylindrical reticulated shell

Fig. 5 shows the model of a typical double-layer cylindrical reticulated shell structure, with the span 35 m, length 60 m, and rise 4 m. The members of the structure are all made of steel tube with the section ϕ95.0×4.0 mm and elastic modulus 2.0×10^5 N/mm^2. The structural damping ratio is 0.02 and the additional distributed mass of the structure is 200 kg/m^2. As shown in Fig. 5, totally 39 MR dampers are laid along the bolded line of the structural model with the maximum damping force 200 kN. The location and number of the dampers are determined according to the comparison of several common-used empirical layout schemes for dampers (same for the numerical examples in section 4.2 and section 4.3). The EL-Centro earthquake wave with the peak value amplitude (PGA) 400 gal is input into the structure along x-direction, and the PGA of y-direction and z-direction are reduced by 15% and 35%. The semi-active control method presented in this paper are adopted to

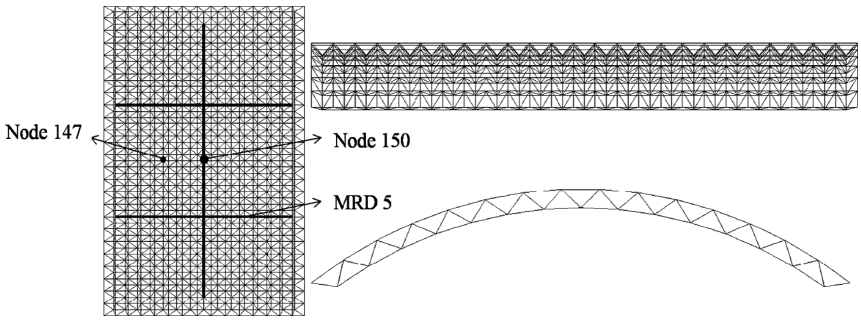

Fig. 5 Structural model of the double-layer cylindrical reticulated shell structure

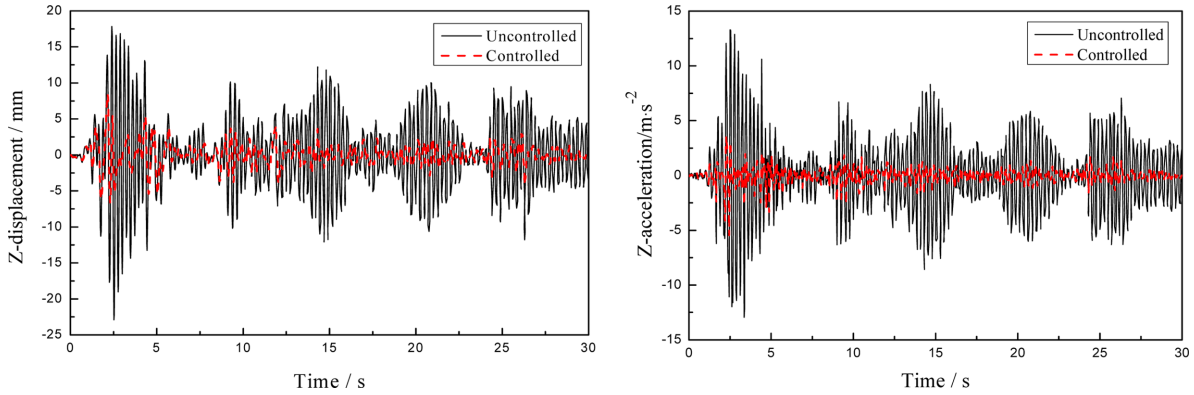

Fig. 6 Displacement and acceleration of node 150

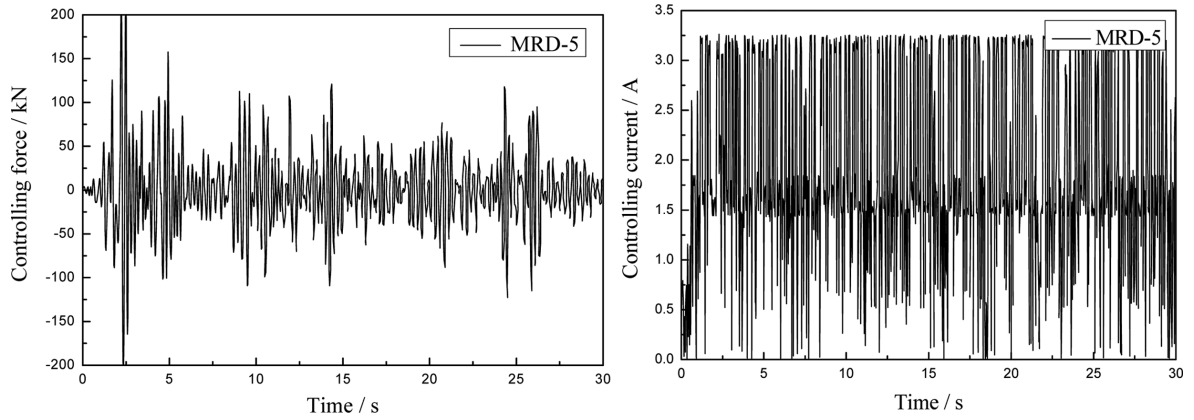

Fig. 7 Controlling force and current of damper MRD-5

controlled the structure on the Matlab/Simulink platform. Two nodes (147 and 150) and one MR damper (MRD5) are selected to show the analytical results.

The *z*-direction displacement, acceleration of the Node 150 and the controlling force, current of MRD-5 are shown in Figs. 6 and 7. It can be seen that in the whole vibration process, the response of the controlled structure is always less than the one of the uncontrolled structure, showing that the semi-active control strategy can steadily controlled the double-layer cylindrical reticulated shell structure under three-dimensional earthquake excitation. As shown in Fig. 7, the real-time feedback from controlling force to current can be simulated by INN model, which can provide the accordance for the controlling terminal in actual engineering.

To evaluate the controlling effect of MR dampers, the peak value control effect parameter β_1 and root-mean-square (RSM) control effect parameter β_2 are defined as

$$\beta_1 = \frac{y_u^P - y_c^P}{y_u^P} \times 100\% \tag{24}$$

$$\beta_2 = \frac{y_u^{RSM} - y_c^{RSM}}{y_u^{RSM}} \times 100\% \tag{25}$$

Table 1 Control effect of the double-layer cylindrical reticulated shell

node	direction of freedom	displacement / mm						acceleration /m·s^{-2}					
		peak value			RSM value			peak value			RSM value		
		y_u^P	y_c^P	β_1 (%)	y_u^{RSM}	y_c^{RSM}	β_2 (%)	y_u^P	y_c^P	β_1 (%)	y_u^{RSM}	y_c^{RSM}	β_2 (%)
147	x	3.39	1.62	52.20	0.91	0.27	70.30	3.95	1.64	58.40	0.69	0.17	75.36
	y	7.61	1.76	76.90	1.71	0.33	80.70	9.46	1.78	81.20	2.27	0.23	89.87
	z	8.42	2.35	72.10	2.32	0.42	81.90	6.96	2.57	63.00	1.67	0.34	79.64
150	x	6.98	2.93	58.00	1.48	0.52	64.90	5.52	2.32	58.10	1.01	0.25	75.25
	y	7.61	1.69	77.80	1.71	0.38	77.78	9.48	2.50	73.60	2.27	0.33	85.46
	z	22.9	8.47	63.00	4.95	1.58	68.10	13.29	5.47	58.80	3.27	0.69	78.90

Where, y_u^P and y_c^P are the uncontrolled and controlled peak value; y_u^{RSM} and y_c^{RSM} are the uncontrolled and controlled RSM value, respectively.The displacement, acceleration and control effect of Node 147 and Node 150 are shown in Table 1. It can be seen that the structural vibration can be effectively reduced by MR dampers. The maximum and minimum displacement peak value control effect is 77.8% and 52.2%, while the one for acceleration is 81.2% and 58.1%. The RSM control effect is greater than the one for peak value, which is 81.9% for maximum displacement control effect and 89.87% for maximum acceleration control effect.

4.2 Single-layer spherical reticulated shell

Fig. 8 shows the model of a Kewitte-6 type single-layer spherical reticulated shell structure, with the span 50 m, rise 10 m and rise-span ratio is 0.2. The members of the structure are all made of steel tube with the section ϕ133.0×4.0 mm and elastic modulus 2.0×10^5 N/mm^2. The structural damping ratio is 0.02 and the additional distributed mass of the structure is 200 kg/m^2. Totally 127 welded ball nodes and 342 members are adopted. As shown in Fig. 8, MR dampers are laid along the bolded line of the structural model. The El-Centro earthquake wave with the peak value amplitude (PGA) 100 gal and 400 gal are respectively input into the structure along x-direction, and the PGA of y-direction and z-direction are reduced by 15% and 35%. The displacement and acceleration of Node 1 and Node 11 is selected to evaluate the control effect of MR dampers.

The z-direction displacement, acceleration of the Node 1 are shown in Fig. 9 and Table 2 shows the peak value control effect of the single-layer spherical reticulated shell under El-Centro record. It can be seen that the controlled displacement and acceleration are both less than the uncontrolled

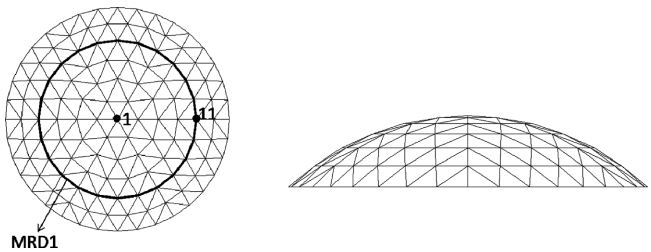

Fig. 8 Structural model of single-layer spherical reticulated shell

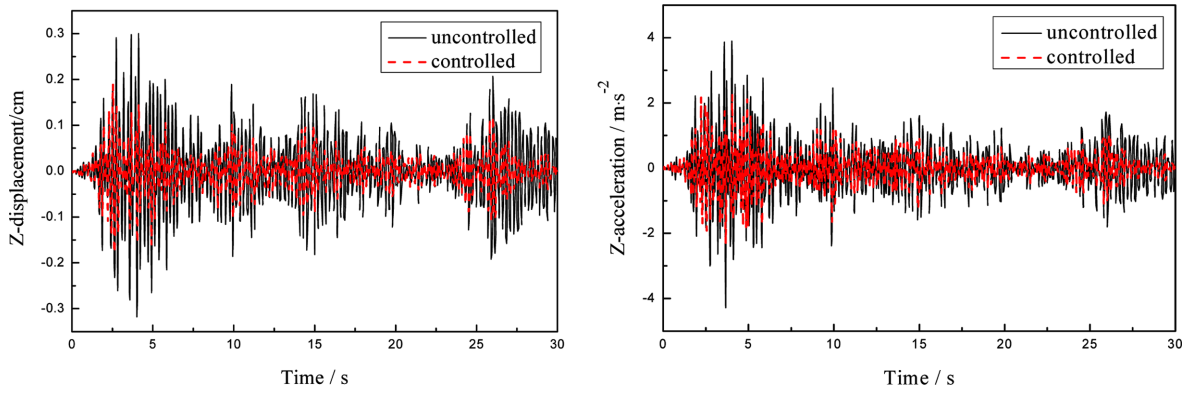

Fig. 9 *Z*-direction displacement and acceleration of Node 1 under 400 gal PGA El-Centro record

Table 2 Control effect of the single-layer spherical reticulated shell under El-Centro record

controlling effect	node	direction of freedom	El-Centro (100 gal)						El-Centro (400 gal)					
			y_u^P	y_c^P	β_1 (%)	y_u^{RSM}	y_c^{RSM}	β_2 (%)	y_u^P	y_c^P	β_1 (%)	y_u^{RSM}	y_c^{RSM}	β_2 (%)
displacement/mm	1	*x*	1.10	0.82	25.50	0.38	0.25	34.20	4.42	3.41	22.90	1.52	1.01	33.55
		y	0.70	0.57	18.60	0.22	0.17	22.70	2.80	2.29	18.20	0.88	0.69	21.60
		z	0.98	0.50	49.00	0.3	0.15	50.00	3.91	2.00	48.80	1.19	0.59	50.42
	11	*x*	2.43	1.69	30.50	0.68	0.45	33.80	9.71	6.74	30.60	2.70	1.82	32.60
		y	0.74	0.65	12.20	0.20	0.15	20.00	2.96	2.58	12.80	0.89	0.67	24.72
		z	3.30	2.25	31.80	0.91	0.61	33.00	13.21	8.99	31.90	3.65	2.46	34.50
acceleration/m·s^{-2}	1	*x*	0.61	0.49	21.00	0.21	0.13	38.09	2.46	1.94	21.00	0.84	0.54	35.70
		y	0.40	0.35	13.90	0.13	0.10	23.07	1.61	1.39	13.80	0.52	0.39	25.00
		z	1.11	0.69	38.50	0.29	0.15	48.30	4.45	2.74	38.40	1.17	0.63	46.15
	11	*x*	1.54	1.07	30.30	0.42	0.25	40.48	6.14	3.86	37.20	1.67	1.02	38.92
		y	0.52	0.45	13.30	0.14	0.11	21.43	2.07	1.80	13.40	0.57	0.45	21.05
		z	2.06	1.53	25.80	0.57	0.35	38.60	8.26	6.13	25.80	2.28	1.42	37.72

ones. The maximum displacement and acceleration control effect are 49% and 38.5% for peak value, 50.42% and 48.3% for RSM value. The *x*-drection and *z*-direction control effect is better than the *y*-direction one, since the *y*-direction response is distinctly less than the other two direction responses. The LQR optimal control strategy is a linear optimal algorithm based on the global stage of the system. The basic principle is that when the system deviates from the balance state, the controlling force is determined based on the minimum enery target to make the system recovering to the balance state. Therefore, the optimal controlling force is more influenced by the *x*-direction and *z*-direction resoponses, and then the *y*-direction control effect is relatively small.

Compared with the numerical example in section 4.1 and section 4.3, the control effect of single-layer spherical reticulated shell is relatively smaller. There are two possible reasons. First, the spherical reticulated shell has greater spatial effect for its grid layout, while the cylindrical reticulated shell and arch-truss are more close to plane arch structure (which can be seen that the vertical displacement of mid-span node are distinctly larger than the horizontal displacement for cylindrical shell and arch-truss). Therefore, the spherical reticulated shell possesses more complex spatial vibration modes and

is more difficult to achieve greater control effect. On the other hand, the MR damper layout in this paper is an empricial scheme. Actually, the location and number of MR dampers could have great influence on the control effect, which need to be optimized using appropriate method in the funture study.

As shown in Table 2, the control effect under 100 PGA and 400 PGA El-Centro recored is very similar, shows that the semi-active control has stable control effect for the single-layer spherical reticulated shell structure under different PGA earthquake excitation.

4.3 Cable suspended arch-truss structure

Cable suspended arch-truss structure is a new type of long-span steel structure consisting of strut, high stress strand and the arch-truss. It could reduce the steel consumption and increase the spanning ability by full exerting the advantages of the arch structure and prestressed cable. The cable suspended arch-truss structure of Harbin International Exhibition Center is taken as an engineering example in this paper. The oblique drawing of the computing model and the position of the dampers was shown in Fig. 10. The span of the structure is 128 m. The cable consists of ϕ39×7 mm prestressed strands, and the elasticity modulus is 1.95×10^5 N/mm. The latticed section is adopted in the arch truss, shown in Fig. 11. The top, bottom and web chords are made of circular seamless steel pipe, in which totally 11 kinds of sections are adopted. The strut is also made of circular seamless steel pipe. The section of strut is ϕ328×8.0 mm, the space between struts is 9.3 m, and the elasticity modulus of struts is 2.0×10^5 N/mm^2. The sag of the cable is 3.7 m. The rise of the arch is 11.7 m. The height of the arch section is 2.6 m. The double-direction (*X*-direction and *Y*-direction) Taft earthquake wave excitation with 100 PGA and 400 PGA are applied to the structure. Considering the coordinated influence of two directions, the PGA at Y-direction is reduced by 35%. The results are shown in Figs. 12 and 13. The displacement, velocity and controlling effect of node 1, 18 and 110 are listed in Table 3.

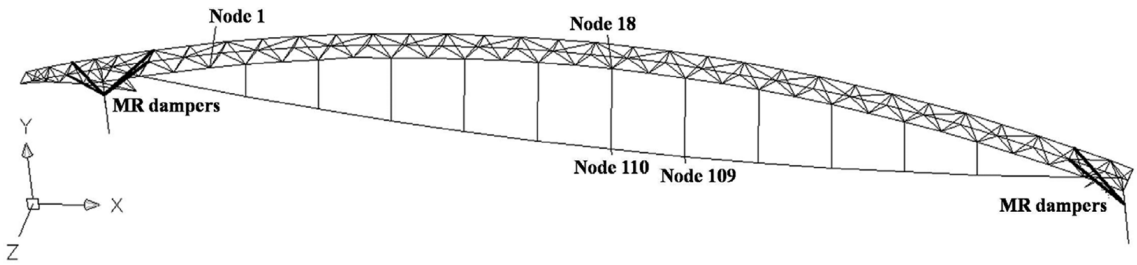

Fig. 10 The cable-arch structure model and the damper location

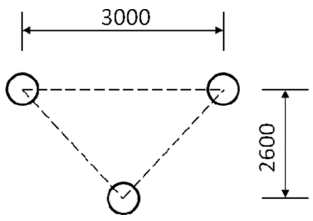

Fig. 11 Cross section of arch truss (unit: mm)

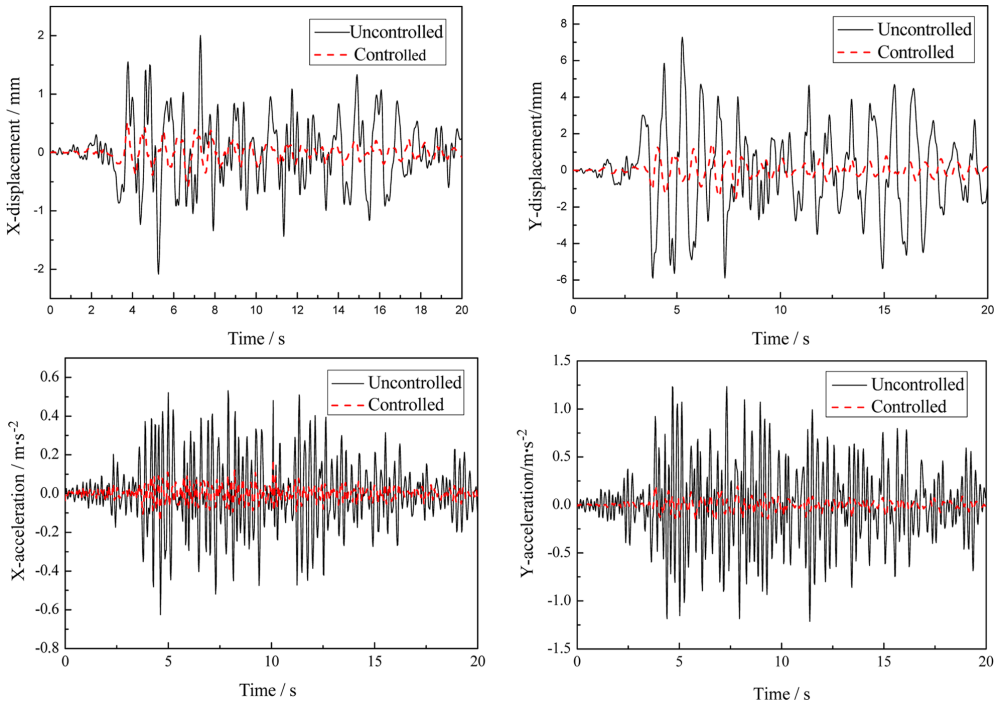

Fig. 12 Displacement and acceleration time-history of node 1 (100PGA Taft record)

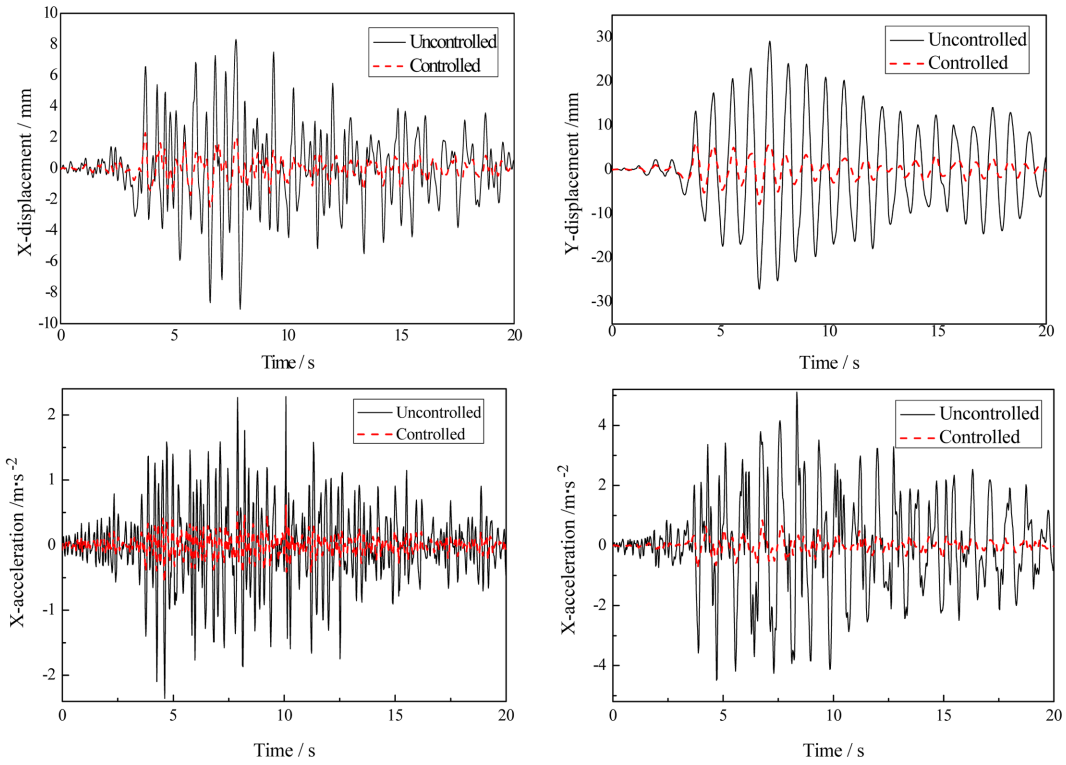

Fig. 13 Displacement and acceleration time-history of node 1 (400PGA Taft record)

Table 3 Displacement and acceleration responses of the structure under Taft record

controlling effect	node	direction of freedom	Taft (100 gal)						Taft (400 gal)					
			y_u^P	y_c^P	β_1 (%)	y_u^{RSM}	y_c^{RSM}	β_2 (%)	y_u^P	y_c^P	β_1 (%)	y_u^{RSM}	y_c^{RSM}	β_2 (%)
displacement/mm	1	x	2.12	0.61	71.23	0.56	0.14	75.00	8.32	2.31	72.24	2.48	0.64	74.20
		y	7.34	1.63	77.79	2.30	0.45	80.4	29.12	6.25	78.54	10.52	2.15	79.56
	18	x	3.92	1.31	66.58	1.04	0.30	68.27	15.54	5.32	65.77	4.63	1.47	68.25
		y	13.11	8.43	35.70	4.11	2.33	43.30	56.61	33.6	40.61	20.45	11.57	43.42
	110	x	1.75	0.74	57.71	0.46	0.17	63.04	6.72	2.83	57.89	2.00	0.78	61.00
		y	13.42	8.57	36.14	4.21	2.37	43.71	57.57	34.1	40.65	20.80	11.76	43.46
acceleration/m·s^{-2}	1	x	0.61	0.22	63.93	0.17	0.04	76.47	2.28	0.62	72.81	0.58	0.15	74.14
		y	1.26	0.19	84.92	0.39	0.05	87.18	5.11	0.85	83.37	1.56	0.21	86.54
	18	x	0.96	0.42	56.25	0.27	0.08	70.37	3.28	0.95	71.04	0.83	0.23	72.29
		y	1.22	0.68	44.26	0.38	0.18	52.63	4.73	1.22	74.21	1.44	0.30	79.20
	110	x	0.73	0.27	63.01	0.21	0.05	76.20	3.10	0.70	77.42	0.78	0.17	78.21
		y	1.21	0.74	38.84	0.37	0.20	45.94	4.64	1.57	66.16	1.41	0.39	72.34

To evaluate the work state of the prestressed cable under the earthquake excitation, the strand stress variation $\Delta\sigma$ is analyzed, which is computed as following

$$\Delta\sigma = E \times \frac{\Delta l}{l} = E \times \frac{\sqrt{(x_{110}-x_{109})^2+(y_{110}-y_{109})^2}}{l} \tag{26}$$

Where, E is the elastic modulus of the strand; Δl is the axial deformation of the strand; x_i, y_i are the x-direction and y-direction displacement respectively of ith node.

Substitute the displacement result to Eq. (25), the time-history of strand stress variation can be obtained as shown in Fig. 5. The maximum strand stress variation is shown in Table 2.

As shown in Figs. 12 and 13 and Table 3, the semi-active control strategy can reduce the displacement and velocity response effectively. The maximum displacement and acceleration control effect are 78.54% and 84.92% for peak value, while 80.4% and 87.18% for RSM value. For the node near the support (Node 1), the y-direction control effect is relatively better than the x-direction control effect,

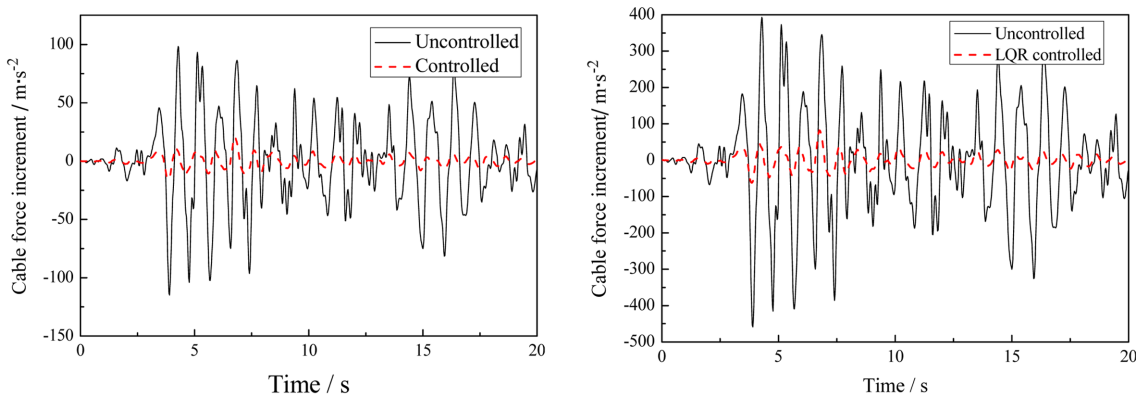

(a) 100gal PGA Taft (b) 400gal PGA Taft

Fig. 14 Strand stress variation time-history of prestressed cable

Table 4 Maximum prestressed stress increment of the strand in the cable

$\Delta\sigma_{max}$ (MPa)	Taft (100 gal)		Taft (400 gal)	
	uncontrolled	controlled	uncontrolled	controlled
	114.7	21.0	440.0	82.0

while the opposite is true for the node near the middle span. This is mainly because that the vertical control force of MR dampers has more direct influence on the nodes near supports. Moreover, as shown in Table 3, the displacement control effect under 100 gal and 400 gal Taft record is very similar, while the acceleration control effect exists distinct error, showing that the semi-active control has stable displacement control effect for the cable suspended arch-truss structure, while the acceleration control effect increase with the intensity of the earthquake excitation.

From Fig. 14 and Table 4, the control strategy can reduce the strand stress variation effectively, ensuring that the cable would not be destroyed or relaxed under the earthquake excitation. The peak value decrease of the strand stress variation is 82% and 81% respectively under 100 gal and 400 gal Taft wave, showing the similar strand stress control effect for earthquake excitations with different PGA.

5. Conclusions

The proposed semi-active control strategy for long-span reticulated structures can determine the optimal spatial control force by using the LQR and Hrovat controlling algorithm, as well as the real-time controlling current of the damper solved by the MBM (modified Bingham model) and INN (inverse neural network). Numerical examples show that the semi-active control strategy can control the displacement and acceleration effectively for three typical long-span reticulated structural systems, including the double-layer cylindrical reticulated shell, single-layer spherical reticulated shell and cable suspended arch-truss. The displacement control effect under the earthquake excitation with different PGA is similar, while for the cable suspended arch-truss, the acceleration control effect increase distinctly with the earthquake excitation intensity. In different vibration direction, the displacement and acceleration control effect may exist distinct difference for the different vibration character of different structures. For the cable suspended arch-truss, the strand stress variation can also be effectively reduced by the MR dampers, which is very important for this kind of structure to ensure that the cable would not be destroyed or relaxed.

6. Future work

Although the numerical analysis in this papaer shows the effectiveness of proposed semi-active control algorithm using MR dampers for long-span reticulated steel structures, some further researches should be conducted and emphasized in future. First, structural control experiments need to be carried out for some typical long-span reticulated steel structures to further verify the semi-active control effect. Besides, since the large amount of members in long-span reticulated steel structures, there are a huge number of damper layout schemes for long-span reticulated steel structure. The suitable method to optimize the location and number of MR dampers need to be figured out according to both the control effect and economical objective.

Acknowledgements

This research is sponsored by "Jiangsu Province Natural Science Foundation of China" (BK2010428), "Fresh Teacher Research Foundation of Chinese Education Ministry" (20090092120017), and "A Project Funded by the Priority Academic Program Development of Jiangsu Higher Education Institutions" (PAPD). The support is gratefully acknowledged.

References

Bitaraf, M., Ozbulut, O.E., Hurlebaus, S. and Barroso, L. (2010), "Application of semi-active control strategies for seismic protection of buildings with MR dampers", *Eng. Struct*., **32**(10), 3040-3047.

Dominguez, A., Sedaghati, R. and Stiharu, I. (2008), "Modeling and application of MR dampers in semiadaptive structures", *Comput. Struct*., **86**(3-5), 407-415.

Erkus, B., Abe, M. and Fujino, Y. (2002), "Investigation of semi-active control for seismic protection of elevated highway bridges", *Eng. Struct*., **24**(3), 281-293.

Fan, F., Cao, Z.Y. and Shen, S.Z. (2010), "Elasto-plastic stability of single-layer reticulated shells", *Thin. Wall. Struct*., **48**(10-11), 827-836.

Huang, H.W., Sun, L.M. and Jiang, X.L. (2012), "Vibration mitigation of stay cable using optimally tuned MR damper", *Smart Struct. Syst*., **9**(1), 35-53.

Iwata, M., Fujita, M. and Wada, A. (1999), "Energy absorbing mechanism for space frame support", *Proceedings of the 2nd World Conference on Structural Control*, Kyoto, Japan.

Jung, H.-J., Jang, J.-E., Choi, K.M. and Lee, H.J. (2008), "MR fluid damper-based smart damping systems for long steel stay cable under wind load", *Smart Struct. Syst*., **4**(5), 697-710.

Kim, I.H., Jung, H.J. and Kim, J.T. (2011), "Numerical investigation of an MR damper-based smart passive control system for mitigating vibration of stay cables", *Struct. Eng.Mech*., **37**(7), 443-458.

Lopez, Ai., Puente, I. and Serna, M. (2007), "Numerical model and experimental tests on single-layer latticed domes with semi-rigid joints", *Comput. Struct*., **85**(7-8), 360-374.

Michel, B. (1998), "Performance of steel bridges during the 1995 Hyogoken-Nanbu (Kobe, Japan) earthquake: a north american perspective", *Eng. Struct*., **20**(12), 1063-1078.

Motohiko, Y. and Lu, G. (1996), "Vibration control of large space structure using TMD system", *Proceedings of the International IASS Conference*, Beijing, China.

Onoda, J., Oh, H.U. and Minesugi, K. (1996), *Semi-active vibration suppression of truss structures by electro-rheological fluid damper*, Collection of Technical Papers-AIAA/ASME/ASCE/AHS Structures, Structural Dynamics & Materials Conference.

Saitoh, M. and Okada, A. (1999), "The role of string in hybrid string structure", *Eng. Struct*., **21**(8), 756-769.

Shen, Z.Y. and Li, Y.Q. and Luo, Y.F. (2004), "Stability of single-layer reticulated shells", *Int. J. Steel Struct*., **4**, 289-300.

Wu, M. (2008), "Analytical method for the lateral buckling of the struts in beam string structures", *Eng. Struct*., **30**(9), 2301-2310.

Wu, W.J. and Cai, C.S. (2010), "Cable vibration control with a semi-active MR damper-numerical simulation and experimental verification", *Struct. Eng. Mech*., **34**(5), 611-623.

Xue, W.C. and Liu, S. (2009). "Design optimization and experimental study on beam string structures", *J. Constr. Steel Res*., **65**(1), 70-80.

Yang, M.G., Chen, Z.Q. and Hua, X.G. (2011), "An experimental study on using MR damper to mitigate longitudinal seismic response of a suspension bridge", *Soil Dyn. Earthq. Eng*., **31**(8), 1171-1181.

Ying, Z.G., Ni, Y.Q. and Ko, J.M. (2009). "A semi-active stochastic optimal control strategy for nonlinear structural systems with MR dampers", *Smart Struct. Syst*., **5**(1), 69-79.

Zhang, Y.G. and Ren, G.Z. (2001), "A practical method on seismic response controlled double layer cylindrical lattice shell with variable stiffness members", *Proceedings of the IASS Symposium*, Nagoya, Japan.